Oil & Gas Science and Technology – Rev. IFP Energies nouvelles (2016) **71**, 48

DOI: 10.2516/ogst/2015043

Zn(II), Mn(II) and Sr(II) Behavior in a Natural Carbonate Reservoir System. Part II: Impact of Geological CO_2 Storage Conditions

B. Auffray[1], B. Garcia[1]*, C.-P. Lienemann[2], L. Sorbier[2] and A. Cerepi[3]

[1] IFP Energies nouvelles, 1-4 avenue de Bois Préau, 92852 Rueil-Malmaison - France
[2] IFP Energies nouvelles, Rond-point de l'échangeur de Solaize, BP 3, 69360 Solaize - France
[3] EA 4592 G&E, ENSEGID, Université de Bordeaux, 1 allée F. Daguin, 33607 Pessac Cedex - France
e-mail: baptiste.auffray@beicip.com; baptiste.auffray@gmail.com - bruno.garcia@ifpen.fr
charles.lienemann@ifpen.fr - loic.sorbier@ifpen.fr - adrian.cerepi@ipb.fr

* Corresponding author

Abstract *— Some key points still prevent the full development of geological carbon sequestration in underground formations, especially concerning the assessment of the integrity of such storage. Indeed, the consequences of gas injection on chemistry and petrophysical properties are still much discussed in the scientific community, and are still not well known at either laboratory or field scale. In this article, the results of an experimental study about the mobilization of Trace Elements (TE) during CO_2 injection in a reservoir are presented. The experimental conditions range from typical storage formation conditions (90 bar, supercritical CO_2) to shallower conditions (60 and 30 bar, CO_2 as gas phase), and consider the dissolution of the two carbonates, coupled with the sorption of an initial concentration of 10^{-5} M of Zn(II), and the consequent release in solution of Mn(II) and Sr(II). The investigation goes beyond the sole behavior of TE in the storage conditions: it presents the specific behavior of each element with respect to the pressure and the natural carbonate considered, showing that different equilibrium concentrations are to be expected if a fluid with a given concentration of TE leaks to an upper formation. Even though sorption is evidenced, it does not balance the amount of TE released by the dissolution process. The increase in porosity is clearly evidenced as a linear function of the CO_2 pressure imposed for the St-Emilion carbonate. For the Lavoux carbonate, this trend is not confirmed by the 90 bar experiment. A preferential dissolution of the bigger family of pores from the preexisting porosity is observed in one of the samples (Lavoux carbonate) while the second one (St-Emilion carbonate) presents a newly-formed family of pores. Both reacted samples evidence that the pore network evolves toward a tubular network type.*

Résumé — Comportement du Zn(II), Mn(II) et Sr(II) au sein d'un système réservoir carbonate naturel. Partie II : impact des conditions de stockage géologique de CO_2 — Aujourd'hui encore, quelques points essentiels limitent le développement industriel de la séquestration géologique du carbone dans des formations souterraines, en particulier celui concernant l'évaluation de l'intégrité du stockage. En effet, les conséquences de l'injection de gaz sur la chimie et les propriétés pétrophysiques sont encore beaucoup discutées au sein de la communauté scientifique, et doivent être mieux comprises tant à l'échelle de laboratoire que sur le terrain.
Dans cet article, le résultat d'une étude expérimentale de mobilisation d'éléments traces suite à une injection de CO_2 dans un réservoir est présenté. Les conditions expérimentales étudiées représentent

des conditions équivalentes à celles d'un stockage typique de formation (90 bar, CO_2 supercritique) jusqu'à des conditions peu profondes (60 et 30 bar, le CO_2 étant sous forme gazeuse), et considèrent la dissolution des deux carbonates, couplées avec la sorption de Zn(II) dont la concentration initiale est de 10^{-5} M, ainsi que la dissolution de Mn(II) et Sr(II).
L'étude présente le comportement spécifique de chaque élément par rapport à la pression et le carbonate naturel considéré, montrant que des concentrations différentes d'équilibre sont à prévoir si des fuites d'un fluide avec une concentration donnée en éléments traces sont présentes vers une formation supérieure. Et même si le phénomène de sorption est mis en évidence, celui-ci ne contrebalance pas la quantité d'éléments traces relargués par le processus de dissolution. L'augmentation de la porosité est clairement mise en évidence comme une fonction linéaire de la pression de CO_2 imposée pour le carbonate de St-Émilion. Pour le carbonate de Lavoux, cette tendance est confirmée par l'expérience de 90 bar. Une dissolution préférentielle de la plus grande famille de pores de la porosité préexistante est observée dans un des échantillons (carbonate de Lavoux) tandis que le second (carbonate de St-Émilion) présente une famille nouvellement formée de pores, avec une géométrie de type tubulaire.

INTRODUCTION

Some disagreements remain in the scientific community over the consequences of climate change and mean temperature increase (Albritton and Meira Filho, 2001). Even so, the role of CO_2 is now known and accepted: its increasing concentration in the atmosphere (from 280 to 380 ppm over the last two hundred years) is estimated to represent around two-thirds of the enhanced greenhouse effect (Bryant, 1997; IPCC, 2007). The major challenge is to mitigate the extent of climate change by reducing anthropic CO_2 emissions to the atmosphere by stabilizing the CO_2 concentration to twice its pre-industrial concentration (around 550 ppm). To do so, the geological storage of CO_2 has been recognized as a significant possibility (Gale *et al.*, 2004; Hepple and Benson, 2005; Holloway, 1997). Coal beds and flood basalts are considered potential storage sites (Garcia *et al.*, 2010; McGrail *et al.*, 2006; Schaef *et al.*, 2010), as are oil and gas fields which are well known and characterized, and which also possess the industrial facilities needed for CO_2 storage (Garcia *et al.*, 2012). But the structures that offer the largest potential for CO_2 geological storage are saline aquifers, as they are widely distributed throughout the globe in sedimentary basins.

Geological storage in saline aquifers involves the injection of SuperCritical CO_2 (SC-CO_2) into porous and permeable layers in the deep subsurface. The long-term storage of CO_2 implies multiple mechanisms:

① structural trapping (CO_2 is trapped by geological structures and buoyant rise);
② capillary trapping as a residual phase in small pores;
③ CO_2 dissolution into the brine (solubility trapping) and reaction with the host rock minerals to form ionic species (ionic trapping);
④ trapping as mineral phases as CO_2 reacts with the host rock and solution.

These reactions are slow but represent the most stable form of CO_2 trapping. The safety of the trapping increases with these different processes (Gaus, 2010). In this article, the focus is on steps ③ and ④ presented above, in the case of a natural carbonate reservoir system. The dissolution of the CO_2 in the water/brine implies many consequences for both the chemistry and the petrophysics of the host formation. The main process is the dissolution of calcite due to the pH decrease that follows the CO_2 dissolution in the aqueous phase. But this dissolution also means that all the species that were originally trapped in the mineral phase are solubilized and therefore able to be displaced by the natural or induced aquifer flux. Indeed, a large number of elements are present at variable concentrations in a carbonate reservoir rock and aquifer (Chadwick *et al.*, 2006).

As SC-CO_2 is injected into the aquifer, chemical interactions occur that lead to a pH drop of a few units and to the dissolution, mobilization and re-precipitation of metals and other rock-forming elements. This ability of the brine to leach metals from the aquifer rocks was evidenced in several articles (Czernichowski-Lauriol *et al.*, 2006; Emberley *et al.*, 2005; Fischer *et al.*, 2010; Gunter *et al.*, 1997; Kharaka *et al.*, 2006, 2009; Rempel *et al.*, 2011; Wigand *et al.*, 2008). This study aims to investigate the behavior of some divalent cations by examining dissolution, precipitation and sorption processes in conditions relevant for CO_2 storage. Indeed, most studies existing in literature are mainly simulation studies based on incomplete databases (Krupka *et al.*, 2010). It also aims to complete the chemical investigations with a petrophysical approach in order to estimate the consequences of CO_2 injection for the transport properties of a formation.

1 MATERIALS AND METHODS

1.1 Samples

The natural carbonates used are the Lavoux and St-Emilion carbonates. They were chosen for their composition (more

than 95% of calcite and quartz) and for their homogeneity. More details on these samples and their preparation can be found in another paper (Auffray *et al.*, 2016).

1.2 Solid Characterization

The analytical methods and techniques used for the initial characterization of the carbonate powders are the same as those described in the previous article (Auffray *et al.*, 2016). The chemical composition is analyzed by coupled X-Ray Diffraction (XRD) and Rock-Eval 6 to obtain the phases present, and ICP-MS analysis for Trace Elements (TE) content. The morphology and petrophysical investigations of the samples are carried out with Scanning Election Microscopy (SEM), BET Specific Surface Area (SSA) and mercury injection. Local Zn enrichment into the carbonate grains is investigated by electron-probe microanalysis. For more details, see Auffray *et al.* (2016). Porosimetry data are obtained using a *Micromeritics* Model 9420 Autopore III Instrument. According to the theoretical basis defined by Washburn (1921) and developed by other authors (Li and Wardlaw, 1986; Lowell and Shields, 1984; Tsakiroglou and Payatakes, 1990; van Brakel, 1981), the porous medium is modeled as a group of cylindrical capillary tubes. The Washburn's equation: $P_c = 4\gamma|\cos\theta|/d_p$, (where P_c is the capillary pressure, d_p is the average pore diameter, γ is the interfacial tension and θ the contact angle between mercury and the pore wall); allows the calculation of petrophysical parameters such as total porosity, distribution of pore throat size, Hg surface area and cavity to throat size ratio. The total porosity is divided into three families according to their pore diameter: macroporosity A (Φ_{MA}: $d_p > 15$ µm), macroporosity B (Φ_{MB}: 0.1 µm < d_p < 15 µm) and mesoporosity (Φ_{meso}: $d_p < 0.1$ µm). The free and trapped porosities (Φ_f and Φ_t respectively) are also calculated from a drainage-imbition cycle.

1.3 Experimental Settings

To investigate the impact of CO_2 geological storage conditions on the behavior of TE in the system $CaCO_3$ - H_2O - CO_2 - NaCl, an hastelloy autoclave (*PAAR*® autoclave) with a sampling feature was used (Fig. 1). To ensure the efficiency of the sampling, a greater quantity of reactants were used: 160 mL of brine along with 4 g of powder to respect the 25 g/L sorbent concentration used in the previous study (Auffray *et al.*, 2016). To ensure that the equilibrium was reached concerning sorption, the experiments lasted around 50 days, with several samplings. The experimental conditions used for those experiments are summarized in Table 1, and temperature and pressure were recorded continuously to detect an eventual leakage from the autoclave. The aqueous samples consisted of 5 mL of solution filtered through a 0.2 µm membrane, and were immediately diluted (factor 2) in an acidified (0.2% HNO_3) solution for subsequent ICP-OES analysis. The mass loss due to sampling all through the experiment did not exceed 16% of the initial liquid mass.

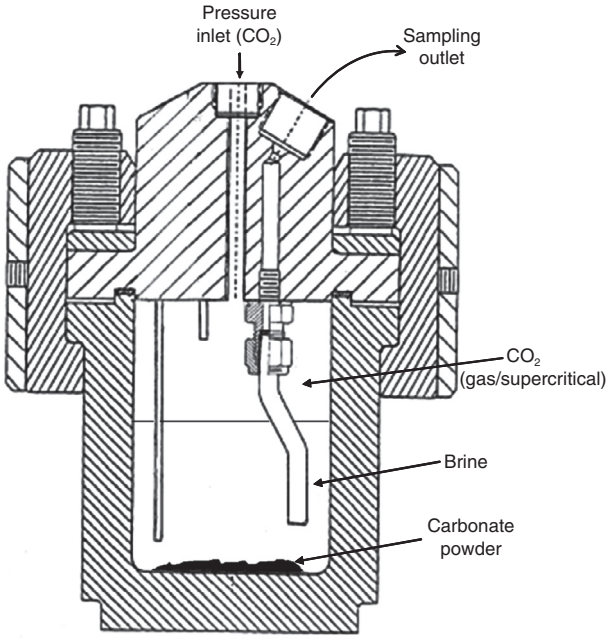

Figure 1

Design of the *PAAR*® autoclave used for the experiments, along with the sampling features.

The Ca(II) concentration at the end of experiments was measured to check the equilibrium of calcite dissolution as no *in-situ* pH measure was possible; the solid phase was also recovered after a Büchner filtration with a 0.2 µm mesh size filter to establish the petrophysical modifications induced by either gas or supercritical CO_2 experimental conditions.

1.4 Numerical Simulations

The geochemical code PHREEQC (Parkhurst and Appelo, 2013) was used with the pitzer.dat database to check the equilibrium of calcite dissolution in the system, as the salinity is around 1.71 M of NaCl (~100 g/L). However, the lack of reliable data on the amount of TE in the powders used, a consequence of the natural heterogeneity of the samples, did not allowed a complete sorption simulation study.

2 RESULTS

2.1 Unreacted Samples

The mineral and chemical composition of the two natural carbonates is available in another article from Auffray *et al.* (2016).

TABLE 1
Initial conditions of dissolution-sorption experiments

Experiment ID	Carbonate	Salinity (g/L NaCl)	Mass of powder (g)	$[Zn(II)]_{aq}$ (mol/L)	Temperature (°C)	Pressure CO_2 (bar)	CO_2 phase
Lav30	Lavoux	100	4.0020	10^{-5}	40	30	Gas
Lav60	Lavoux	100	4.0036	10^{-5}	40	60	Gas
Lav90	Lavoux	100	3.9997	10^{-5}	40	90	Supercritical
StEm30	St-Emilion	100	4.0021	10^{-5}	40	30	Gas
StEm60	St-Emilion	100	4.0012	10^{-5}	40	60	Gas
StEm90	St-Emilion	100	3.9926	10^{-5}	40	90	Supercritical

2.2 Chemistry

2.2.1 Equilibrium in the Systems

The steady state in the system was checked by measuring the concentration of Ca(II) in solution at the end of the experiments. The values obtained are presented in Table 2, along with the simulated values and the corresponding error. The Lavoux carbonate experiments present a good match with the simulation data, with less than 5% difference between the experimental and simulated values. Concerning the St-Emilion carbonate, the experimental data also fits very well with the simulated values, with a slightly high value measured for the 30 bar experiment (~7.3% of difference). Depending on the CO_2 pressure in the system, between 0.5 and 0.7 g of the initial calcite mass (~4 g) is dissolved, according to the final Ca(II) concentration measured in solution. The simulated values obtained with the database minteq.v4.dat are given in the last two columns of Table 2, to evidence the impact of the database on such simulations where high salinity experiments are concerned. The results show a strong overestimation of the dissolution process at such salinity and pressures with this last database.

2.2.2 Divalent Cation Behavior and Scavenging Effect

The behaviors of Zn(II), Mn(II), and Sr(II) are presented considering the evolution of their aqueous concentration with respect to time (Fig. 2-4).

In the experiments carried out with the Lavoux carbonate (Fig. 2a), the Zn(II) concentration shows an increasing trend when the pressure is fixed at 30 bar. At higher pressures (60 and 90 bar), a slight decrease of the Zn(II) concentration is observed, which means that the Zn(II) released by dissolution is adsorbed on the carbonate. The variations in concentration observed in those cases, correlated with the dissolution process, show that Zn(II) does not interact the same way with the Lavoux carbonate according to the pressure conditions. For the experiment carried out with the St-Emilion carbonate, three very different behaviors are evidenced. At 30 bar, sorption happens at a very slow

TABLE 2
Results of final Ca(II) concentration measurements and corresponding simulations with both databases. The error is calculated as the difference between measured and simulated concentration divided by the simulated value, and multiplied by 100

Experiment	Measured	Dissolved calcite, calculated	Pitzer.dat	Error, relative to pitzer simulations	Minteq.v4.dat	Error, relative to minteq.v4 simulations
	$[Ca(II)]_{eq}$ (mol/L)	(g)	$[Ca(II)]_{eq}$ (mol/L)	(%)	$[Ca(II)]_{eq}$ (mol/L)	(%)
Lav30	0.03579	0.57	0.0364	−1.7	0.04525	−20.9
Lav60	0.04227	0.68	0.0414	2.1	0.06127	−31.0
Lav90	0.04163	0.67	0.0432	−3.6	0.07335	−43.2
StEm30	0.03376	0.54	0.0364	−7.3	0.04525	−25.4
StEm60	0.04176	0.67	0.0414	0.9	0.06127	−31.8
StEm90	0.04136	0.66	0.0432	−4.3	0.07335	−43.6

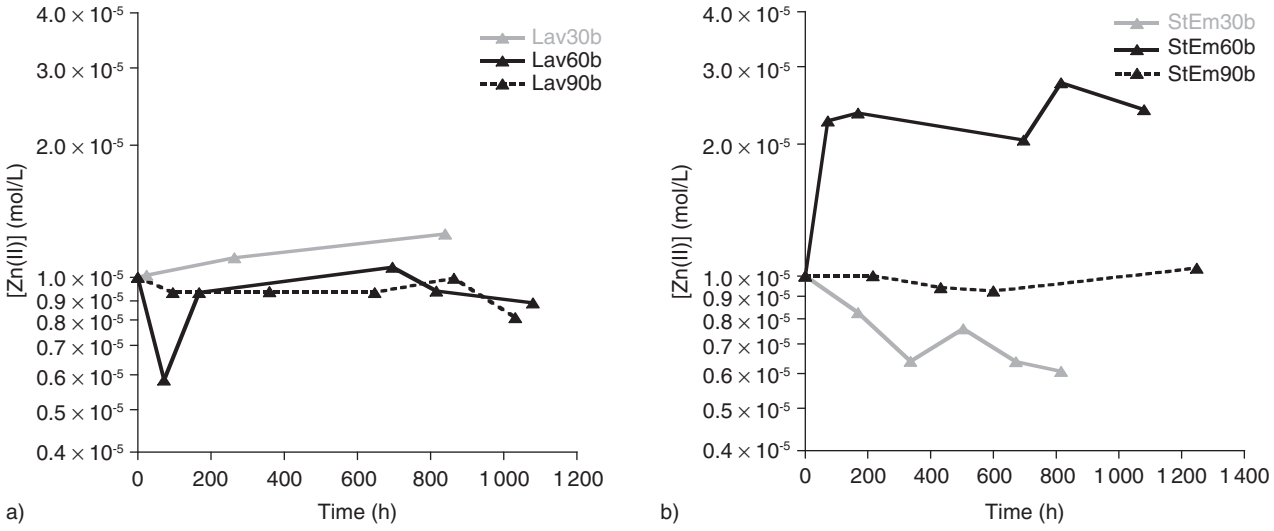

Figure 2

Zinc concentration as a function of time. a) Experiments run with the Lavoux carbonate at 30 bar (full line, grey), 60 bar (full line, black), and 90 bar (dotted line, black). b) Experiments run with the St-Emilion carbonate at 30 bar (full line, grey), 60 bar (full line, black), and 90 bar (dotted line, black). Error bars are comprised within symbol size.

rate with a decrease of about 40% of the Zn(II) concentration. At 60 bar, the end concentration measured is close to twice the initial Zn(II) concentration, implying a strong Zn (II) release from the St-Emilion carbonate due to calcite dissolution. In supercritical conditions, the Zn(II) concentration is nearly constant all through the experiment. As dissolution of the natural carbonate occurs at such pressure, there is a nearly perfect balance between the Zn(II) sorbed and the Zn(II) released due to calcite dissolution.

The study of Mn(II) concentration behavior (Fig. 3) shows that where the Lavoux carbonate is concerned, the difference between the three pressure conditions is very slight, as evidenced for Zn(II). However, as no Mn(II) is initially present in solution, the conclusions are not the same concerning the sorption of this element. Indeed the amount of Mn(II) released is supposed to be nearly equal at 30 and 90 bar, and higher at 60 bar, according to calcite dissolution data. However, the final Mn(II) concentrations at 60 and 90 bar are lower than the one at 30 bar, meaning that sorption is stronger when the CO_2 pressure increases. For the St-Emilion carbonate experiments, the Mn(II) concentration increase is more important, in agreement with the higher Mn(II) content in the St-Emilion carbonate, but the end concentrations indicate different behaviors according to pressure. At 30 bar, the end Zn(II) concentration is nearly the same as for experiment with the Lavoux carbonate. At higher pressures, the end concentrations indicate a lower amount of Mn(II) sorbed at 90 bar than at 60 bar. This trend is well correlated with the trend of Zn(II) in experiments with the same carbonate.

The behavior of Sr(II) concentration over time (Fig. 4), seems to evidence a pressure dependent sorption equilibrium, which can be correlated with the dissolution effect. Indeed, for both carbonates, the lower equilibrium concentration is observed at 30 bar, the next one is at 90 bar and the higher equilibrium value is at 60 bar: this observation is consistent with the amount of calcite dissolved given in Table 2. However this apparent pressure dependence for the final Sr(II) concentration has also to be correlated with the varying of the number of available sorption sites, which vary according to the dissolution of calcite. In all of these experiments, the time to reach the end concentrations is between 100 and 200 h, this variability relying on the sampling dates selected. An apparent organization according to pressure is evidenced for the three elements of interest in the St-Emilion carbonate experiments, observed also with Sr(II) for Lavoux carbonate experiments, which will be discussed later in this article.

2.3 Solid Phase Evolution

2.3.1 Petrophysical Consequences

The petrophysical changes following the different pressure conditions are presented in this section (Fig. 5, 6), based on mercury injection data (Tab. 3).

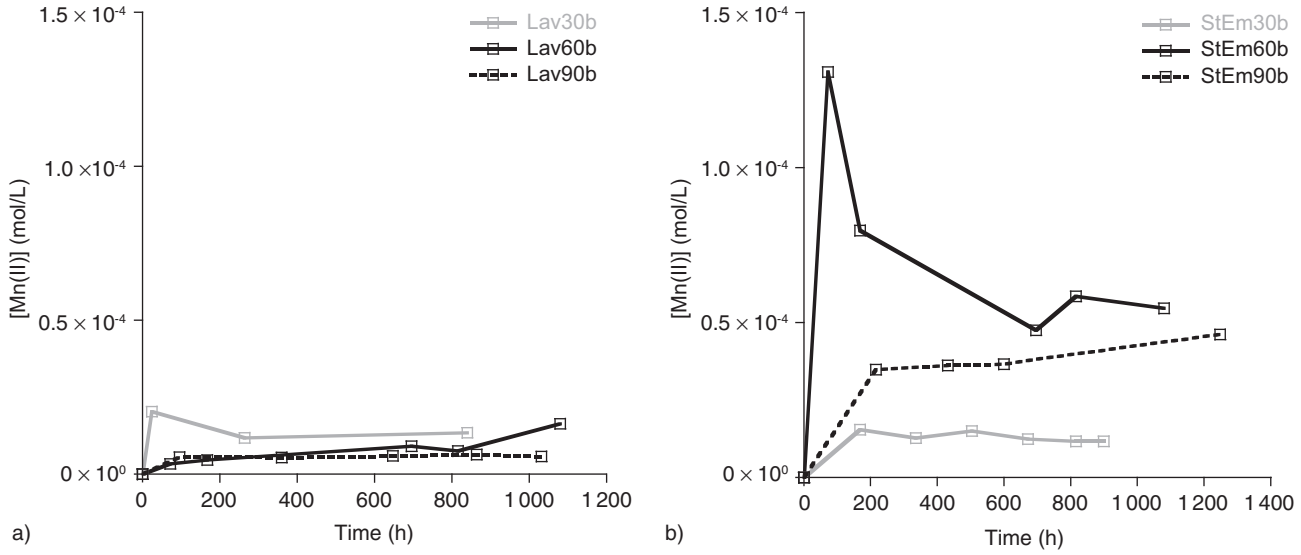

Figure 3

Manganese concentration as a function of time. a) Experiments run with the Lavoux carbonate at 30 bar (full line, grey), 60 bar (full line, black), and 90 bar (dotted line, black). b) Experiments run with the St-Emilion carbonate at 30 bar (full line, grey), 60 bar (full line, black), and 90 bar (dotted line, black). Error bars are comprised within symbol size.

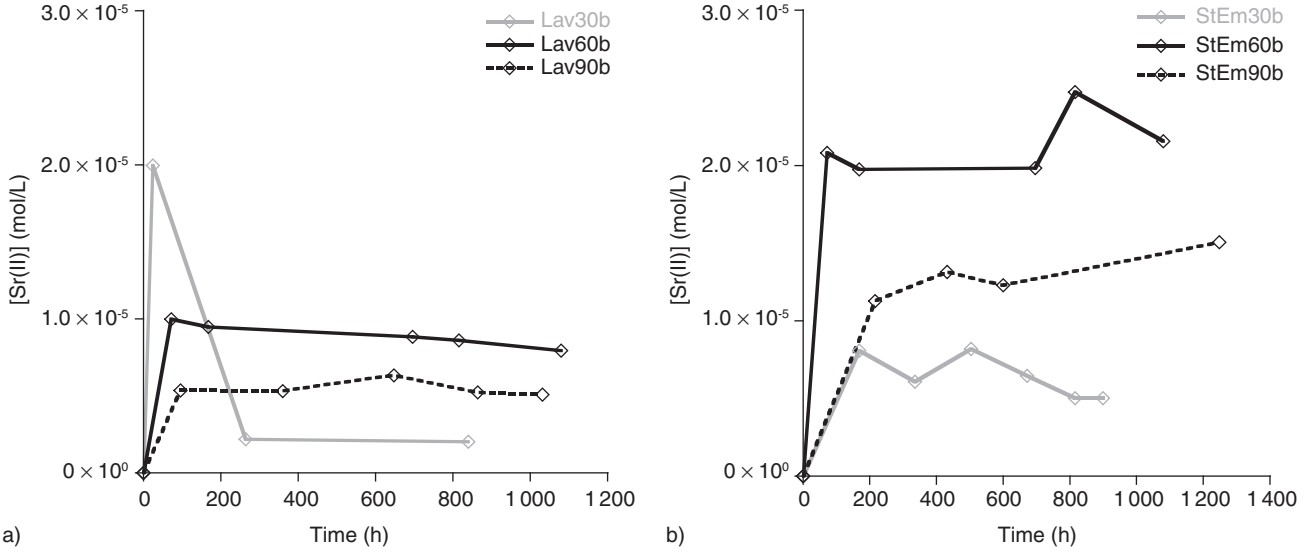

Figure 4

Strontium concentration as a function of time. a) Experiments run with the Lavoux carbonate at 30 bar (full line, grey), 60 bar (full line, black), and 90 bar (dotted line, black). b) Experiments run with the St-Emilion carbonate at 30 bar (full line, grey), 60 bar (full line, black), and 90 bar (dotted line, black). Error bars are comprised within symbol size.

2.3.1.1 The Lavoux Carbonate

On the Lavoux carbonate porosity distribution curves (Fig. 5a), the characterization of the initial powder is plotted with the reacted powders dataset. A progressive evolution is evidenced with the increasing pressure conditions of the experiments. The initial curve presents a double porosity characterized by two main families, FLav_1 (d_p below 10 µm) and FLav_2 (d_p over 10 µm). When reacted at

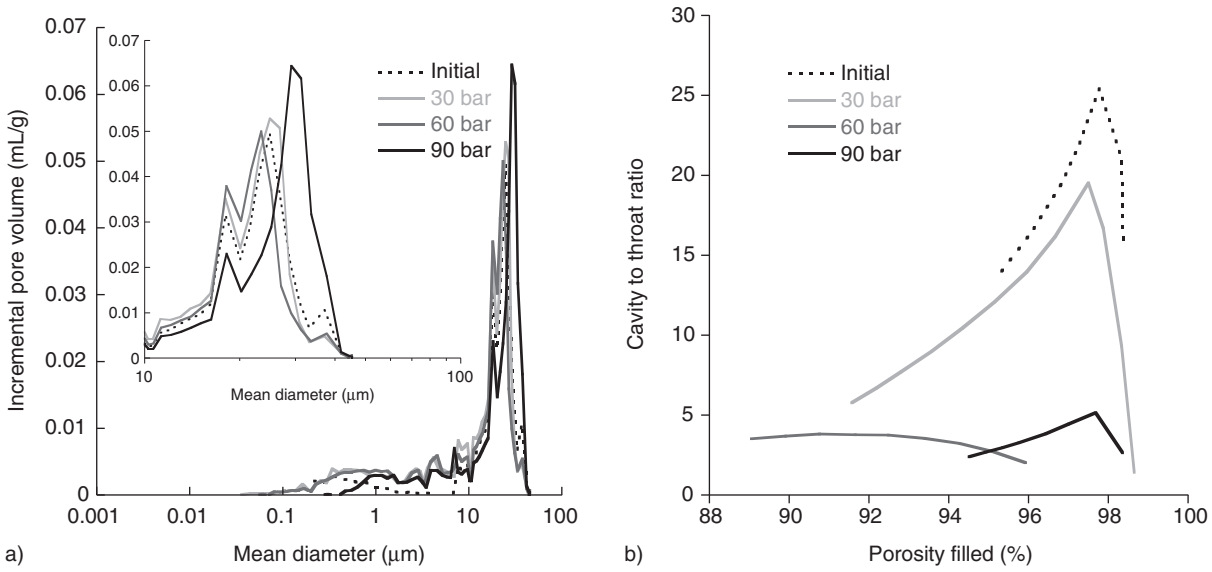

Figure 5

Lavoux carbonate mercury injection data comparison for initial carbonate, and reacted powder at 30, 60, and 90 bar of CO_2. a) Incremental pore volume as a function of the mean pore diameter. A zoom of the 10-100 µm range is added on this figure. b) Cavity to throat ratio evolution with respect to porosity filling.

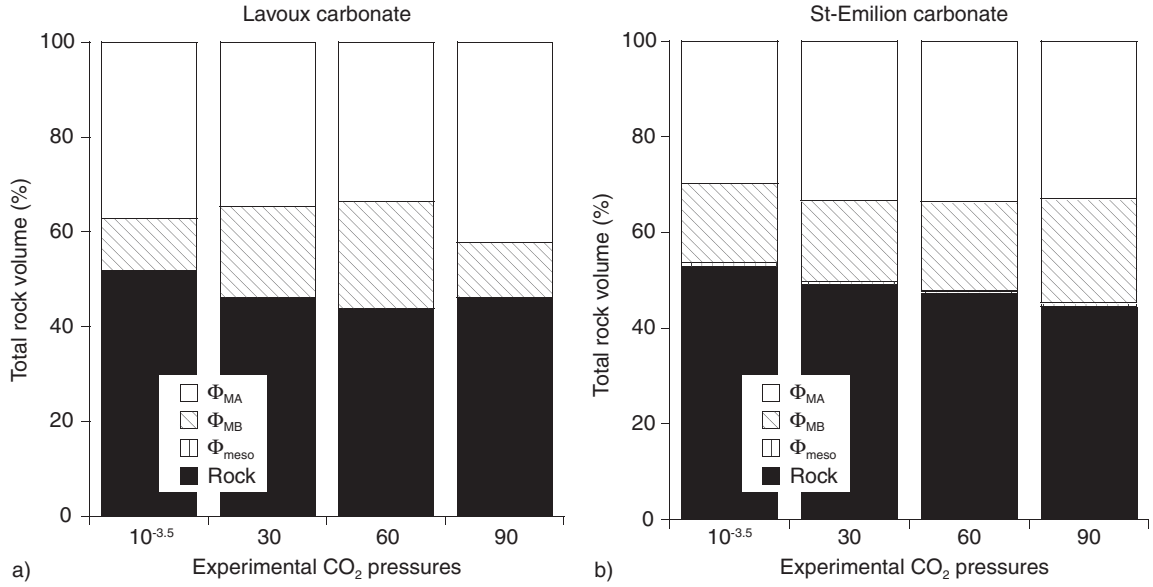

Figure 6

Comparative evolution of the families composing the total porosity of the Lavoux a) and the St-Emilion b) carbonates with the CO_2 pressure conditions of the experiments (atmospheric, 30, 60 and 90 bar). Three families of porosity are represented: macroporosity A (white), macroporosity B (diagonal lines) and mesoporosity (vertical lines), along with the rock fraction (black).

30 bar pressure, no major impact is evidenced on the FLav_1 family, but the FLav_2 family presents a larger peak, slightly shifted towards higher mean diameters. With a 60 bar pressure, the peak of the first family of pores is higher, while the second is slightly shifted towards smaller pore diameters. This shift to the left of the FLav_2 pore family is a side effect

TABLE 3
Results of SSA measurements and mercury injection

Experiment	SSA	Φ	Φ increase	Φ_{MA}	Φ_{MB}	Φ_{meso}	Φ_f	Φ_t	Asp	HD (4V/A)
	(m^2/g)	(%)	(%)	(%)	(%)	(%)	(%)	(%)	(m^2/g)	(nm)
Lav30	0.54	54.07	5.7	34.68	19.21	0.18	4.67	49.40	0.683	2.753
Lav60	0.75	64.63	16.3	41.17	23.32	0.14	7.49	57.14	0.578	2.858
Lav90	0.92	53.85	5.5	42.17	11.68	0.00	2.95	50.90	0.187	9.408
StEm30	1.30	50.89	3.8	33.43	16.80	0.66	4.06	46.83	0.912	1.737
StEm60	1.06	52.33	5.2	33.81	18.53	0.36	3.15	49.18	/	/
StEm90	1.53	55.47	8.4	34.95	19.75	0.78	3.05	52.42	0.974	1.703

of the global increase of the pore volume observed in the 20-25 µm range of mean diameter. Finally, at 90 bar pressure, the first family presents a much lower peak than in the three other conditions, correlated with a clear shift in the FLav_2 pore family towards 30 µm of mean diameter. The pressure increase effect on this carbonate can be summarized as: with CO_2 as gas phase, the dissolution increases the volume available behind the 20-25 µm mean pore diameter range; while the supercritical CO_2 mainly increases the diameter of the bigger pores. The curves plotted in Figure 5b illustrate this preferential dissolution effect by showing the evolution of the cavity to throat ratio with respect to porosity filling. As pressure increases, the trend shows that this ratio diminishes from a mean value of 20 down to a mean value of 5: dissolution tends to homogenize the porous media and to create tubular shaped pores.

The data in Table 3 indicates a 5% to 15% increase of the total porosity in the Lavoux carbonate (by comparison with the initial characterization data, Auffray *et al.*, 2016), depending on the pressure conditions. Concerning macroporosity A (Φ_{MA}: d_p > 15 µm), the contribution of this family to the total porosity value decreases with the increasing CO_2 pressure in the experiments (from about 77% to 60%). Macroporosity B (Φ_{MB}: 1 µm < d_p < 15 µm) makes an increasing contribution to the total porosity when CO_2 pressure increases, and mesoporosity (Φ_{meso}: 1 µm > d_p) is very slightly impacted by the experimental conditions. The measure of the SSA indicates an increasing function with pressure. For a better representation of what happens for each family of porosity, Figure 6 summarize these results for both carbonates.

2.3.1.2 The St-Emilion Carbonate

The evolution of the pore size distribution of the St-Emilion carbonate (Fig. 7a) is more complicated. Initially it presents one pore family, referred as FStEm_1 (d_p below 10 µm), but the CO_2 pressure conditions and related dissolution lead to the creation of a second pore family, FStEm_2 (20 µm < d_p < 30 µm). With a 30 bar CO_2 pressure, this second family has a peak as high as the one of FStEm_1. At 60 bar, the available pore volume after this range of pore size increases (higher peak) and shifts slightly towards lower diameters. Lastly, the 90 bar experiment evidences that the two main families of mean pore diameters represent almost the same pore volume. With this carbonate, the possible creation of a new pore family is evidenced. Considering the cavity to throat ratio (Fig. 7b), from the initial mean value of 17, the 30 and 60 bar of CO_2 conditions decrease this value to something around 8, and at 90 bar, this mean ratio is about 11. As for the Lavoux carbonate, the increasing CO_2 pressure seems to homogenize the porous media towards a cylindrical shape.

The total porosity (Tab. 3) increases almost linearly with pressure, from its initial value of 47% to 51% at 30 bar, 52.3% at 60 bar and 55.5% at 90 bar. The available volume behind macroporosity A increases about 3% of the total porosity regardless the pressure applied, while macroporosity B increases with CO_2 pressure. As for the Lavoux carbonate, the mesoporosity is only slightly impacted by the dissolution process (Fig. 6b).

2.3.2 Specific Surface Area

The variations of the SSA of each sample with respect to the imposed experimental conditions are presented in Table 3. The Lavoux carbonate evolves from its initial value of 0.60 m^2/g (Auffray *et al.*, 2016) to 0.54, 0.75 and 0.92 m^2/g for experiments carried out at 30, 60 and 90 bar of CO_2 respectively. The variation measured at 30 bar of CO_2 is comprised within the incertitude range, so no variation of the SSA is evidenced in this experiment. But clearly, at 60 and 90 bar, the dissolution of the carbonate is correlated with an increase of the specific surface area of 25% and 53% respectively. The SSA measures of the St-Emilion carbonate powders also evolved from the initial value of 1.20 m^2/g. The 30 bar CO_2 pressure leads to a 1.30 m^2/g SSA (8% more) and 1.06 m^2/g (about 12% less) for 60 bar of CO_2

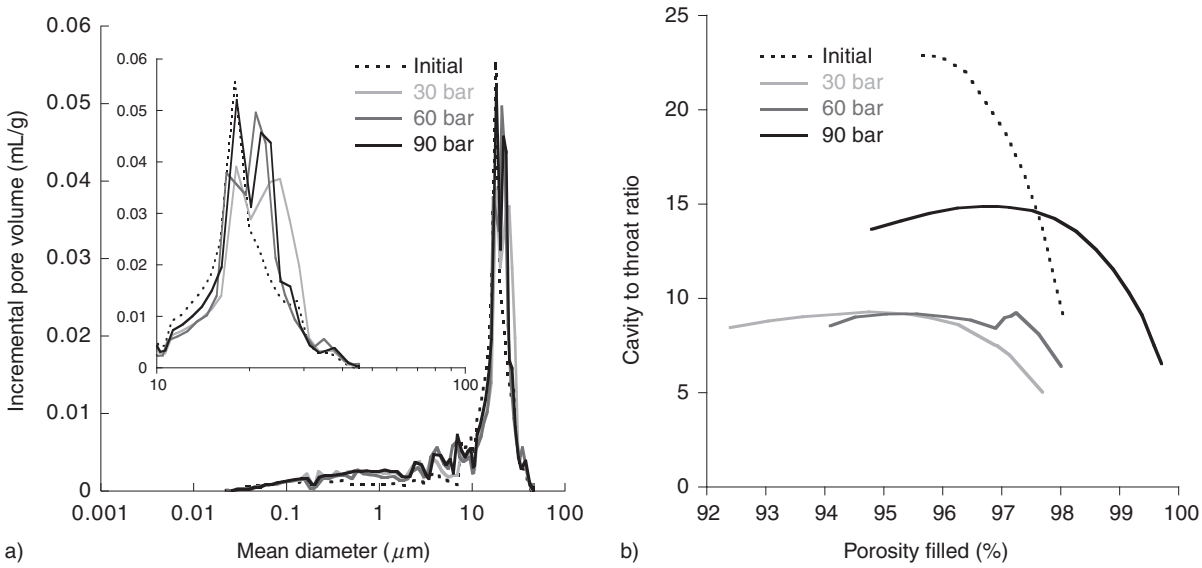

Figure 7

St-Emilion carbonate mercury injection data comparison for initial carbonate, and reacted powder at 30, 60, and 90 bar of CO_2. a) Incremental pore volume as a function of the mean pore diameter. A zoom of the 10-100 μm range is added on this figure. b) Cavity to throat ratio evolution with respect to porosity filling.

pressure: those values are closely within the 10% error range of the measure; but at 90 bar it increases up to 1.53 m²/g (an increase of ~27%). The dissolution of the St-Emilion carbonate is not clearly correlated to an increase of the SSA, except at a CO_2 pressure of 90 bar.

2.3.3 Microprobe

The microprobe analysis of the reacted powders did not evidence any zinc enrichment of the periphery of the grains (data not shown). All the measures (about 15 grains for each experiment) indicated that the zinc content was always below the detection limit of about 75 ppm.

3 DISCUSSION

3.1 Equilibrium of the System and TE Behavior

CO_2 injection under the supercritical phase is considered the easiest way to inject this molecule underground, because in this state it has both the density of a liquid and the viscosity of a gas (IPCC, 2007). With these experiments (30, 60 and 90 bar at 40°C) coupled with PHREEQC simulations, we evidence that the gas and supercritical states of CO_2 in high salinity conditions (~100 g/L NaCl) are well managed by the numerical code, as stated by other studies (Krupka *et al.*, 2010). This is at least proved for CO_2 pressures up to 90 bar.

Thus, it is possible to simulate accurately the dissolution of calcite in conditions relevant for CO_2 geological storage (supercritical state, high salinity), but the system of interest in this article is more complex in terms of composition: the numerous TE that are solubilized and especially their fate are of major interest. As discussed in another article (Auffray *et al.*, 2016), the Pitzer database used for high salinity simulations does not contain the specific parameters for Zn(II), Mn(II), Sr(II) and their related species. This lack of thermodynamic data has already been pointed by several studies (Bateman *et al.*, 2005; Bentham and Kirby, 2005; Bethke, 2008; Gaus *et al.*, 2008; Kaszuba *et al.*, 2003; Xu *et al.*, 2004), but never concerning the TE released in the system by mineral dissolution. An accurate simulation tool for combined dissolution, precipitation and sorption phenomenon is still to be developed.

The importance of thermodynamic data concerning TE is emphasized in this article by focusing on the evolution with time of the TE in the aqueous phase. Another study (Viswanathan *et al.*, 2012) points out that in the specific context of their study, As is mobilized in the aqueous phase and that, despite sorption and/or reprecipitation, an amount of this As remains in solution. What we observe in the experiments presented here demonstrates that this mobilization effect also exists for elements such as zinc, manganese and

strontium in the natural carbonate context studied here. After the initial increase of TE concentration following the dissolution of calcite, sorption occurs in the systems that lead to a reduced amount of element in solution. For example the steady-state concentration of Mn(II) in solution at 60 bar of CO_2 for the St-Emilion carbonate is a third of the initial concentration measured after the initial pulse (Fig. 3b). Another important result enlightened in this study is the specific behavior of the TE with respect to the natural carbonate used. Indeed, Zn(II) behavior is not the same if one considers the Lavoux or the St-Emilion carbonates experiments, whatever the pressure considered. A probable explanation could be the impact of the petrophysical properties of the different samples, coupled with their respective evolution to the CO_2 pressures.

The last result evidenced by this study is the specific sorption behavior of the TE with respect to pressure. Indeed, the Ca(II) concentration in solution, related to calcite dissolution, indicates nearly the same quantities of dissolved calcite at 60 and 90 bar. One would expect the same end concentration for each TE in solution, but this is absolutely not the case: the end concentration is always higher at 60 than at 90 bar, and this occurs whatever the TE considered. This result can be discussed in the light of the parameters relevant for the sorption phenomena, including the SSA (Dzombak and Morel, 1990; Sverjensky, 2003; Zachara *et al.*, 1991, 1988). The variation of this parameter could explain the difference observed by comparing values from Table 2 and Figures 2-4. Despite the same dissolved masses measured, the SSA increases much more for experiments carried out at 90 bar. To our knowledge, this was never reported in the literature, probably due to the fact that all the previous sorption studies were carried out only under atmospheric pressure and strictly controlled conditions to prevent the dissolution from being of major impact on the results (Martin-Garin *et al.*, 2003; Tertre *et al.*, 2010; Villegas-Jiménez *et al.*, 2009; Zachara *et al.*, 1988, 1991).

This discussion evidences well the actual lack of knowledge concerning the behavior of TE in a CO_2 geological storage context, especially if one wants to assess the safety of a storage site regarding the possible contamination by TE. It also points out the other subject still discussed in the community (Gaus *et al.*, 2008), which is the link between the injection of SC-CO_2, the chemical reactions that will follow and the evolution of the petrophysical properties of the host formation.

3.2 Linking Chemistry and Petrophysics

Indeed, as presented by several other studies (Bachaud *et al.*, 2011), a key point to better understand the consequences of SC-CO_2 injection in a given formation is to obtain more information about the linked evolution of chemistry and petrophysical properties in the system. To do so, a parallel between the calcium concentration in the aqueous phase and the petrophysical variations is discussed in this part, based on the values presented in Table 3 and Figures 5-7. No correlation is observed between the total porosity increase and the calcite mass dissolved in the experiments, and a first explanation of this discrepancy is the use of powders in these experiments. Indeed, the dissolution process occurs on both the external and internal (porosity) parts of the grains, while mercury injection gives only access to pores that have a diameter below 44 µm. This means that all the variations in the external structure of the grains are not taken into account via mercury injection analyses. Still, the impact of dissolution on porosity is specifically studied by considering the different families that compose the total porosity.

The results of the experiments show that dissolution impacts mainly the two pore families Φ_{MA} and Φ_{MB} as depicted by Figure 6. By comparison with the pore size distributions of the two initial carbonates (Fig. 5, 7), this observation is coherent. Indeed, the main variations correspond to the diameter range 10-100 µm. This observation agrees well with preferential dissolution zones evidenced by Bachaud *et al.* (2011) in cap-rock samples, particularly for the Lavoux carbonate. The St-Emilion carbonate, though, is useful in evidencing the fact that this preferential dissolution is not always valid. With the increasing CO_2 pressures (30, 60 and 90 bar) a new family of pores appears around 20 µm of pore diameter. To complete this discussion on the impact of dissolution on the porous media, the cavity to throat ratio indicates, coherently with the previous discussion, that the porous network is homogenized by dissolution. This is true for both carbonates, as their cavity to throat ratio decreases by a factor 4 approximately. Dissolution tends to dissolve throats and create a tube-like porous network. This result is expected in the case of flow through experiments, but it seems also to be the case for the powders used in these experiments.

3.3 Extrapolation to a CO_2 Storage Context and Possible Leakages from a Reservoir Formation

In the case of a real storage site, other specificities must be kept in mind: first, the fact that the rock formation does not have the same properties as powders relative to sorption and reactivity (Qafoku *et al.*, 2013), and then that the space (vertical and horizontal) and time scales considered are much wider. Indeed, in this article the focus is on impacts of a CO_2 pressure of 30, 60 and 90 bar, which corresponds roughly to 300, 600 and 900 m depths, depending on the regional conditions. At these depths, the mobilization of TE contained in host formations is evidenced, and potentially balanced by the sorption and/or reprecipitation

phenomena, depending on the carbonate rock. The modifications of the petrophysical properties evidence a probable increase in the transport properties of the formation. But to complete the study of CO_2 impacted zones by a leakage, as discussed in other papers (Harvey *et al.*, 2013; Little and Jackson, 2010; Viswanathan *et al.*, 2012), the subsurface environment and shallow aquifers are also of importance. Results are presented on this particular aspect of the impact of the CO_2 underground storage on water quality in another paper from the authors (Auffray *et al.*, 2016), that deals with the influx of a brine loaded with a given concentration of Zn(II) in a carbonate reservoir. The last aspect to investigate is the impact on the vadose zone: a field study was carried out in an old quarry of the St-Emilion village (France) but with no aspect concerning the behavior of TE in those specific hydrologic conditions (Cohen *et al.*, 2013; Garcia *et al.*, 2013; Le Roux *et al.*, 2013; Loisy *et al.*, 2013).

CONCLUSIONS

A leakage of fluid (gas and/or brine) from the storage formation is a major uncertainty concerning the safety assessment of a CO_2 geological storage project. The consequences can vary a lot, all along the pathway that brine and gas follow as they leak from the storage formation to an upper one, as evidenced in this paper. Considering sorption and dissolution, pressure dependent behaviors for the TE considered, we evidence in this paper chemical variations in the fluid composition, but also modifications of the structure of the porous media, and consequently on the flow properties of the concerned formation. The increase of TE concentration in solution is evidenced, and sorption does not balance this release in solution in most cases, despite an available SSA that is much higher than the SSA that will be available in a real storage site. Even in a real storage context, the dissolution is supposed to be lower than what we observe in those experiments, due to aquifer flow, non negligible amounts are thought to be mobilized (Viswanathan *et al.*, 2012; Zheng *et al.*, 2009; Wigand *et al.*, 2008) when one considers the huge volume of injected CO_2 that is envisaged (Lu *et al.*, 2012; Rempel *et al.*, 2011). To fill this gap in our knowledge, more experimental studies must be carried out to understand more the real behavior of those TE in CO_2 storage conditions.

Where closer aquifers of potable water resources are concerned, the debate is still open to know whether a CO_2 leakage would be a benefit or an issue (Harvey *et al.*, 2013), but concerning at least the three species studied here, Zn(II) for example could become toxic with the concentrations observed, as this element reaches concentrations around 10^{-8} M (WHS, 2011). Nevertheless, the precipitation of metal carbonate minerals, an aspect not evidenced in this study, must be considered in a real storage site far from the injection well, as CO_2 density and concentration decrease, leading to possible incorporation of metals elements due to precipitation of secondary phases (Gunter *et al.*, 1997; Xu *et al.*, 2010, 2004).

ACKNOWLEDGMENTS

B. Auffray is thankful to Michel Chardin for his help in managing the *PAAR*® autoclave experimental settings and the associated procedures; Frederic Neyret-Martinez and Nathalie Texier for their availability during the ICP-AES analysis campaigns. The authors also thank the two anonymous reviewers for their contribution to improving this paper. This article is part of the PhD thesis of B. Auffray, funded by *IFP Energies nouvelles.*

REFERENCES

Albritton D.L., Meira Filho L.G. (2001) Contribution of Working Group I Third Assessment Report on Intergovernmental Panel on Climate Change, in *Climate Change 2001: the Scientific Basis*, Cambridge, Cambridge Univ. Press, UK and New York, USA.

Auffray B., Garcia B., Lienemann C.-P., Sorbier L., Cerepi A. (2016) Zn(II), Mn(II) and Sr(II) Behavior in a Natural Carbonate Reservoir System. Parti I: Impact of Salinity, Initial pH and Initial Zn(II) Concentration in Atmospheric Conditions, *Oil & Gas Science and Technology* **71**, 47.

Bachaud P., Berne P., Renard F., Sardin M., Leclerc J.P. (2011) Use of tracers to characterize the effects of a CO_2-saturated brine on the petrophysical properties of a low permeability carbonate caprock, *Chemical Engineering Research and Design* **89**, 1817-1826.

Bateman A.S., Kelly S.D., Jickells T.D. (2005) Nitrogen isotope relationships between crops and fertilizer: Implications for using nitrogen isotope analysis as an indicator of agricultural regime, *Journal of Agricultural and Food Chemistry* **53**, 5760-5765.

Bentham M., Kirby G. (2005) CO_2 Storage in Saline Aquifers, *Oil & Gas Science and Technology* **60**, 3, 559-567.

Bethke C.M. (2008) *Geochemical and Biogeochemical reaction modeling*, Cambridge University Press, New York.

Bryant E. (1997) *Climate Process and Change*, Cambridge University Press, Cambridge.

Chadwick A., Noy D., Lindeberg E., Arts R., Eiken O., Williams G. (2006) Calibrating reservoir performance with time-lapse seismic monitoring and flow simulations of the Sleipner CO_2 plume, *Proceedings of the 8th International Conference on Greenhouse Gas Control Technologies*, Trondheim, Norway, June 19-22.

Cohen G., Loisy C., Laveuf C., Le Roux O., Delaplace P., Magnier C., Rouchon V., Garcia B., Cerepi A. (2013) The CO_2-Vadose project: Experimental study and modelling of CO_2 induced leakage and tracers associated in the carbonate vadose zone, *International Journal of Greenhouse Gas Control* **14**, 128-140.

Czernichowski-Lauriol I., Rochelle C., Gaus I., Azaroual M., Pearce J., Durst J. (2006) Geochemical interactions between CO_2, pore-waters and reservoir rocks - Lessons learned from laboratory experiments, field studies and computer simulations, *NATO Science Series IV Earth and Environmental Sciences* **65**, 157-174.

Dzombak D.A., Morel F.M.M. (1990) *Surface Complexation Modeling: Hydrous Ferric Oxide*, Wiley-Interscience, New York.

Emberley S., Hutcheon I., Shevalier N., Durocher K., Mayer B., Gunter W.D., Perkins E.H. (2005) Monitoring of fluid-rock interaction and CO_2 storage through produced fluid sampling at the Weyburn CO_2-injection enhanced oil recovery site, Saskatchewan, Canada, *Applied Geochemistry* **20**, 1131-1157.

Fischer R., Lorenz M., Köhl M., Mues V., Granke O., Iost S., van Dobben H., Reinds G.J., de Vries W. (2010) The condition of forests in Europe, *ICP Forests, 2010 Executive Report*, Hamburg, Germany, and European Commission, Brussels, Belgium.

Gale J.F.W., Laubach S.E., Marrett R.A., Olson J.E., Holder J., Reed R.M. (2004) Predicting and characterizing fractures in dolostone reservoirs: Using the link between diagenesis and fracturing, in *The Geometry and Petrogenesis of Dolomite Hydrocarbon Reservoirs*, Braithwaite C.J.R., Rizzi G., Darke G. (eds), Geological Society (London) Special Publication 235.

Garcia B., Beaumont V., Perfetti E., Rouchon V., Blanchet D., Oger P., Dromart G., Huc A., Haeseler F. (2010) Experiments and geochemical modelling of CO_2 sequestration by olivine: Potential, quantification, *Applied Geochemistry* **25**, 1383-1396.

Garcia B., Hy Billiot J., Rouchon V., Mouronval G., Lescanne M., Lachet V., Aimard N. (2012) A Geochemical Approach for Monitoring a CO_2 Pilot Site: Rousse, France. A Major gases, CO_2-carbon isotopes and Noble Gases Combined Approach, *Oil Gas Science and Technology* **67,** 341-353.

Garcia B., Delaplace P., Rouchon V., Magnier C., Loisy C., Cohen G., Laveuf C., Le Roux O., Cerepi A. (2013) The CO_2-vadose project: Numerical modeling to perform a geochemical monitoring methodology and baseline performance assessment for various geochemical variables (gas flux, gas composition, stable isotopes and noble gases) in the carbonate vadose zone, *International Journal of Greenhouse Gas Control* **14**, 247-258.

Gaus I. (2010) Role and impact of CO_2-rock interactions during CO_2 storage in sedimentary rocks, *International Journal of Greenhouse Gas Control* **4**, 73-89.

Gaus I., Audigane P., André L., Lions J., Jacquemet N., Durst P., Czernichowski-Lauriol I., Azaroual, M. (2008) Geochemical and solute transport modelling for CO_2 storage, what to expect from it? *International Journal of Greenhouse Gas Control* **2**, 605-625.

Gunter W.D., Genetzis T., Rottenfuser Richardson R.J.H. (1997) Deep coalbed methane in Alberta Canada: A fuel resource with the potential of zero greenhouse gas emissions, *Energy Conservation and Management* **38S**, 217-222.

Harvey O.R., Qafoku N.P., Cantrell K.J., Lee G., Amonette J.E., Brown C.F. (2013) Geochemical Implications of Gas Leakage associated with Geologic CO_2 storage - A Qualitative Review, *Environmental Science and Technology* **47**, 23-26.

Hepple R.P., Benson S.M. (2005) Geologic storage of carbon dioxide as a climate change mitigation strategy: performance requirements and the implications of surface seepage, *Environmental Geology* **47,** 4, 576-585.

Holloway S. (1997) An overview of the underground disposal of carbon dioxide, *Energy Conversion and Management* **38**, 193-198.

IPCC (2007) Special Report on Carbon Capture and Storage.

Kaszuba J.P., Janecky D.R., Snow M.G. (2003) Carbon dioxide reaction processes in a model brine aquifer at 200°C and 200 bars: implications for geologic sequestration of carbon, *Applied Geochemistry* **18,** 1065-1080.

Kharaka Y.K., Cole D.R., Hovorka S.D., Gunter W.D., Knauss K.G., Freifield B.M. (2006) Gas-water-rock interactions in Frio Formation following CO_2 injection: Implications for the storage of greenhouse gases in sedimentary basinsn, *Geology* **34**, 577-580.

Kharaka Y.K., Thordsen J.J., Hovorka S.D., Nance H.S., Cole D.R., Phelps T.J., Knauss K.G. (2009) Potential environmental issues of CO_2 storage in deep saline aquifers: Geochemical results from the Frio-I Brine Pilot test, Texas, USA, *Applied Geochemistry* **24**, 1106-1112.

Krupka K.M., Cantrell K.J., McGrail B.P. (2010) Thermodynamic Data for Geochemical Modeling of Carbonate Reactions Associated with CO_2 Sequestration - Literature Review, in *Report PNNL-19766*.

Le Roux O., Cohen G., Loisy C., Laveuf C., Delaplace P., Magnier C., Rouchon V., Cerepi A., Garcia B. (2013) The CO_2-Vadose project: Time-lapse geoelectrical monitoring during CO_2 diffusion in the carbonate vadose zone, *International Journal of Grennhouse Gas Control* **16**, 156-166.

Li Y., Wardlaw N.C. (1986) Mechanisms of Nonwetting Phase Trapping during Imbibition at Slow Rates, *Journal of Colloid and Interface Science* **109**, 473-486.

Little M.G., Jackson R.B. (2010) Potential impacts of leakage from deep CO_2 geosequestration on overlying freshwater aquifers, *Environmental Science and Technology* **44**, 9225-9232.

Loisy C., Cohen G., Laveuf C., Le Roux O., Delaplace P., Magnier C., Rouchon V., Cerepi A., Garcia B. (2013) The CO_2-Vadose Project: Dynamics of the natural CO_2 in a carbonate vadose zone, *International Journal of Greenhouse Gas Control* **14**, 97-112.

Lowell S., Shields J.E. (1984) *Powder Surface Area and Porosity*, Chapman and Hall.

Lu J., Kharaka Y.K., Thordsen J.J., Horita J., Karamalidis A., Griffith C., Hakala J.A., Ambats G., Cole D.R., Phelps T.J., Manning M.A., Cook P.J., Hovorka S.D. (2012) CO_2-rock-brine interactions in Lower Tuscaloosa Formation at Cranfield CO_2 sequestration site, Mississippi, U.S.A., *Chemical Geology* **291**, 269-277.

Martin-Garin A., van Cappellen P., Charlet L. (2003) Aqueous cadmium uptake by calcite: A stirred flow-through reactor study, *Geochimica et Cosmochimica Acta* **67**, 2763-2774.

McGrail B.P., Schaef H.T., Ho A.M., Chien Y.-J., Dooley J.J., Davidson C.L. (2006) Potential for carbon dioxide sequestration in flood basalts, *Journal of Geophysical Research* **111**, B12201.

Parkhurst D.L., Appelo C.A.J. (2013) Description of Input and Examples for PHREEQC Version 3 - A Computer Program for Speciation, Batch-Reaction, One-Dimensional Transport, and Inverse Geochemical Calculations.

Qafoku N.P., Brown C.F., Wang G., Sullivan C., Lawter A.R., Harvey O.R., Bowden M. (2013) Geochemical Impacts of Leaking CO_2 from Subsurface Storage Reservoirs to Unconfined and Confined Aquifers. Report PNNL-22420.

Rempel K.U., Liebscher A., Heinrich W., Schettler G. (2011) An experimental investigation of trace element dissolution in carbon dioxide: Applications to the geological storage of CO_2, *Chemical Geology* **289**, 224-234.

Schaef H.T., McGrail B.P., Owen A.T. (2010) Carbonate mineralization of volcanic province basalts, *International Journal of Greenhouse Gas Control* **4**, 249-261.

Sverjensky D.A. (2003) Standard states for the activities of mineral surface sites and species, *Geochimica et Cosmochimica Acta* **67**, 17-28.

Tertre E., Beaucaire C., Juery A., Ly J. (2010) Methodology to obtain exchange properties of the calcite surface - Application to major and trace elements: Ca(II), HCO_3^-, and Zn(II), *Journal of Colloid and Interface Science* **347**, 120-6.

Tsakiroglou C.D., Payatakes A.C. (1990) A New Simulator of Mercury Porosimetry for the Characterization of Porous Materials, *Journal of Colloid and Interface Science* **137**, 315-339.

van Brakel J. (1981) Mercury Porosimetry: State of the Art, *Powder Technology* **29**, 1-12.

Villegas-Jiménez A., Mucci A., Pokrovsky O.S., Schott J. (2009) Defining reactive sites on hydrated mineral surfaces: Rhombohedral carbonate minerals, *Geochimica et Cosmochimica Acta* **73**, 4326-4345.

Viswanathan H., Dai Z., Lopano C., Keating E., Hakala J.A., Scheckel K.G., Zheng L., Guthrie G.D., Pawar R. (2012) Developing a robust geochemical and reactive transport model to evaluate possible sources of arsenic at the CO_2 sequestration natural analog site in Chimayo, New Mexico, *International Journal of Greenhouse Gas Control* **10**, 199-214.

Washburn E.W. (1921) Note on a method of determining the distribution of pore sizes in a porous material, in *Proceedings of the National Academy of Sciences of the United States of America* **7**, 115-116.

Wigand M., Carey J.W., Schutt H., Spangenberg E., Erzinger J. (2008) Geochemical effects of CO_2 sequestration in sandstones under simulated *in situ* conditions of deep saline aquifers, *Applied Geochemistry* **23**, 2735-2745.

World Health Statistics 2011 World Health Organization.

Xu T., Apps J., Pruess K. (2004) Numerical simulation of CO_2 disposal by mineral trapping in deep aquifers, *Applied Geochemistry* **19**, 917-936.

Xu T., Kharaka Y.K., Doughty C., Freifeld B.M., Dalye T.M. (2010) Reactive transport modeling to study changes in water chemistry induced by CO_2 injection at the Frio-I Brine Pilot, *Chemical Geology* **271**, 3-4, 153-164.

Zachara J.M., Kittrick J.A., Harsh J.B. (1988) The mechanism of Zn^{2+} adsorption on calcite, *Geochimica et Cosmochimica Acta* **52**, 2281-2291.

Zachara J.M., Cowan C.E., Resch C.T. (1991) Sorption of divalent metals on calcite, *Geochimica et Cosmochimica Acta* **55**, 1549-1562.

Zheng L., Apps J.A., Zhang Y., Xu T., Birkholzer J.T. (2009) On mobilization of lead and arsenic in groundwater in response to CO_2 leakage from deep geological storage, *Chemical Geology* **268**, 281-297.

Manuscript submitted in April 2015
Manuscript accepted in November 2015
Published online in April 2016

Cite this article as: B. Auffray, B. Garcia, C.-P. Lienemann, L. Sorbier and A. Cerepi (2016). Zn(II), Mn(II) and Sr(II) Behavior in a Natural Carbonate Reservoir System. Part II: Impact of Geological CO_2 Storage Conditions, *Oil Gas Sci. Technol* **71**, 48.